Princeton Plasma Physics Laboratory

PPPL- 4316

PPPL- 4316

Field Line Resonance at Mercury's Magnetosphere: A Simulation Study

Eun-Hwa Kim, Jay R. Johnson, and Dong-Hun Lee

May 2008

Prepared for the U.S. Department of Energy under Contract DE-AC02-76CH03073.

Princeton Plasma Physics Laboratory
Report Disclaimers

Full Legal Disclaimer

Trademark Disclaimer

PPPL Report Availability

Princeton Plasma Physics Laboratory:

http://www.pppl.gov/techreports.cfm

Office of Scientific and Technical Information (OSTI):

http://www.osti.gov/bridge

Related Links:

U.S. Department of Energy

Office of Scientific and Technical Information

Fusion Links

Field line resonance at Mercury's magnetosphere: A simulation study

Eun-Hwa Kim,[1] Jay R. Johnson,[1] and Dong-Hun Lee,[2]

Abstract. Ultra low frequency (ULF) waves, which are assumed to be standing waves on the field, are observed by the Mariner 10 spacecraft at Mercury. These waves are oscillating at 38% of the proton gyrofrequency. It is well known that the heavy ions, such as Na^+, are abundant in Mercury's magnetosphere. Because the presence of different ion species has an influence on the plasma dispersion characteristics near the ion gyro-frequencies, such relatively high frequencies of magnetospheric eigenoscillations at Mercury require a multi-fluid treatment for the plasma. Thus ULF waves at Mercury may have a distinct difference from typical ULF oscillations at Earth, which are often described in terms of magnetohydrodynamics (MHD). By adopting a multi-fluid numerical wave model, we examine how magnetic eigenoscillations occur in Mercury's magnetosphere. Because protons and sodium ions are the main constituents at Mercury, we assume an electron-proton-sodium plasma in our model. The frequency spectra and time histories of the electromagnetic fields at the ion-ion hybrid (IIH) and cavity resonances are presented. Our results show: (1) The observed ULF waves are likely compressional waves rather than FLR. (2) Resonant absorption occurs at the IIH resonance, thus incoming compressional waves are converted into the IIH resonance. (3) The IIH resonance is strongly guided by the background magnetic field and shows linear polarization in the east-west meridian. (4) Both the Alfvén and the IIH are suggested as a mechanism for FLR at Mercury. (5) The resonance frequency enables us to estimate the local heavy ion concentration ratio.

1. Introduction

During the first encounter with Mercury's magnetosphere, *Russell* [1989] detected a narrow band pulsation with frequency about 0.5 Hz in the night side magnetosphere. Although the signals are preferentially polarized in the magnetic meridian rather than east-west direction, *Russell* [1989] proposed that the pulsation was a standing Alfvén wave along a background magnetic field line (B_0), because the signals are primarily transverse to $\mathbf{B}_0$. Using an electron density of 3cm^{-3} and assuming an electron-proton plasma with the measured field strength, he derived an Alfvén velocity of about 1,000 km/s. With a field line length of about 4,000 km based on a dipole model, *Russell* [1989] estimated that the fundamental frequency of a standing wave on the field line would be about 0.125Hz. Accordingly, the observed 0.5Hz wave could be the fourth harmonic of the fundamental wave. The local proton gyrofrequency ($f_{\text{cH}} = \omega_{\text{cH}}/2\pi$) during the wave event observed by Mariner 10 was 1.31 Hz, and the observed wave frequency was at 38% of f_{cH}. However, because these waves are well outside the MHD frequency range, the MHD approximation is not applicable for these observations.

It is well known that heavy ions are abundant in Mercury's magnetosphere. Plasma sources for Mercury's magnetosphere are the solar wind, supplying H^+ and He^+, as well as sputtering from the planetary surface and subsequent photoionization. The observed sputtered products are O, Na, and K [*Lammer and Bauer*, 1997]. The contributions of ionized K and O to the magnetospheric plasma are negligible compared with that of Na [*Cheng et al.*, 1987]. From analysis of the Na exosphere and Na^+ tracing, *Ip* [1986] and *Cheng et al.* [1987] suggested that Na^+ could make up between 10% and 50% of the magnetospheric ion plasma composition. The abundance of He^+ in Mercury's magnetosphere is still unknown.

Such minor ions can modify the characteristics of the ion gyrofrequency range of plasma waves. Because the observed wave frequency, 0.5 Hz, lies between the local gyrofrequency of protons, 1.31Hz, and sodium, 0.057 Hz, a proper analysis of the oscillations requires a wave model that includes multi-ions [*Othmer et al.*, 1999; *Glassmeier et al.*, 2003, 2004; *Klimushkin et al.*, 2006]. The major issues that can be addressed by a multi-fluid approach are (1) understanding the characteristics of field line resonances (FLR) with frequency the order of the gyrofrequency in multi-ion plasmas and (2) determining the ion composition Mercury's magnetosphere.

When incident compressional MHD waves arrive at a region where the phase speed parallel to $\mathbf{B}_0$ is equal to the local Alfvén speed, the wave energy is transferred to shear Alfvén waves [*Hasegawa et al.*, 1983]. This resonant absorption of MHD waves provides a mechanism for FLRs in Earth's magnetosphere that has been recognized for decades [e.g., *Tamao*, 1965; *Uberoi*, 1972; *Chen and Hasegawa*, 1974; *Southwood*, 1974].

At higher frequency ($f \sim f_{\text{cH}}$), the MHD approximations become invalid and the Alfvén resonance becomes the perpendicular ion cyclotron resonance, which is the frequency modified Alfvén resonance [e.g., *Stix*, 1992]. At the Alfvén resonance, wave energy transfers from the compressional wave to the shear Alfvén wave mode [e.g., *Karney et al.*, 1979; *Winglee*, 1982; *Kim and Lee*, 2003]. The finite f/f_{cH} effect on ULF waves becomes important on the magnetosheath [*Belmont and Rezeau*, 2001], the magnetopause [*Rezeau et al.*, 1989], and laboratory plasma experiments [e.g., *Tsushima et al.*, 1982; *Mitchell et al.*, 2001].

When minor ions are included in the plasma, there are two additional resonances between the gyrofrequencies, a

[1]Plasma Physics Laboratory, Princeton University, Princeton, New Jersey, USA.

[2]Department of Astronomy and Space Science, Kyung Hee University, Kyunggi, Korea

0148-0227/08/$9.00

Buchsbaum-Bers (BB) and an ion-ion hybrid (IIH) resonances. At the IIH resonance, the absorption from the fast Alfvén wave to the resonance occurs [e.g., *Lee et al.*, 2008], and both resonances provide important clues in Earth's ULF waves [e.g., *Johnson et al.*, 1995; *Horne and Thorne*, 1997; *Johnson and Cheng*, 1999; *Lee et al.*, 2008].

Othmer et al. [1999] and *Klimushkin et al.* [2006] derived a necessary condition for resonant mode coupling in multi-ion plasmas which is the same condition as the IIH resonance. They also suggested that the crossover frequency is the preferred frequency for the FLR at Mercury when this frequency is satisfied at the resonance condition. By adopting a two-fluid wave model, *Kim and Lee* [2003] examined the behavior of the Alfvén resonance when $f \sim f_{\rm cH}$ and discussed the implications for waves at Mercury. However, *Southwood* [1997] argued that the observed waves cannot be pure standing Alfvén waves because they have a compressional component and polarization aligned in the north-radial meridian rather than east meridian. Thus it is necessary to further investigate FLRs at Mercury's magnetosphere.

The overall aim of this paper is to consider the FLR phenomena for Mercury's multi-ion plasmas. First, we need to define that the FLR condition at the Mercury. To achieve this goal, we adopt typical plasma parameters on Mercury and perform a wave simulation. We demonstrate that compressional waves can be converted into the IIH resonance linearly when the heavy ion density ratio varies across the magnetic field B_0. These results are compared with previous observational and theoretical work. In addition, we introduce a method of heavy ion density estimation using resonance frequencies. Because the IIH resonance depends on the ratio of ion density to electron density, it enables us to estimate the heavy ion density ratio.

This paper is structured as follows: We briefly describe wave properties in an electron-proton-sodium plasma in Section 2. The resonance conditions and other pure ion-ion effects are also introduced. Section 3 and 4 describe the numerical simulation model and the results obtained from simulations such as wave spectra and time histories of electric and magnetic fields. Time histories of the electromagnetic wave at the resonance location provide direct evidence of resonant absorption at the IIH resonance. In Section 5, we investigate methods to determine the ion density ratio using the IIH and the Alfvén resonance frequencies. The last section contains a brief discussion and the conclusions.

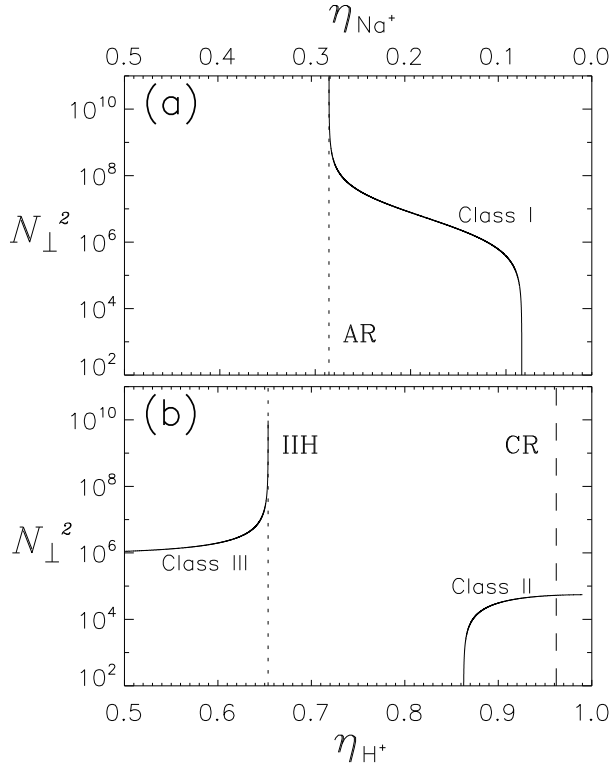

Figure 1. The $n_\perp^2$ dispersion relation using Eq. (3) in an electron-proton-sodium plasmas for (a) $\omega = 0.03\omega_{\rm cH} < \omega_{\rm cNa}$ and (b) $\omega_{\rm cNa} < \omega = 0.2\omega_{\rm cH} < \omega_{\rm cH}$. Wave mode are referred to as Class I, II, and III following to *Rauch and Roux* [1982]. Here the dotted lines are the Alfvén (AR) and the IIH resonances and the dashed line represents the crossover (CR).

2. Waves in multi-ion plasmas

The inclusion of minor ions changes the dispersion of waves in the range of the ion gyrofrequencies [e.g., *Smith and Brice*, 1964; *Young et al.*, 1981; *Rauch and Roux*, 1982]. For $\theta = 0^\circ$, the left-handed (L) polarized branch splits into multiple propagation bands propagating between the ion gyrofrequencies. Each branch has a resonance at the ion gyrofrequencies and an additional cutoff between two ion gyrofrequencies (except for below the heaviest ion gyrofrequency). Conversely, the right-hand (R) mode is nearly unaffected by additional minor ions.

For $\theta = 90^\circ$, there is a splitting of the extraordinary (X) wave branch. The existence of an additional resonance for the X wave was noted by *Buchsbaum* [1960]. This X wave resonance between the ion gyrofrequencies will be referred to as the "Buchsbaum-Bers (BB) resonance",

$$\omega_{\rm bb}^2 = \omega_{\rm c1}\omega_{\rm c2}\left(\frac{\eta_1 M_2 + \eta_2 M_1}{\eta_1 M_1 + \eta_2 M_2}\right), \tag{1}$$

where $\omega_{\rm c}$ is the proton gyrofrequency, $\eta_j = N_j/N_{\rm e}$ the fraction of the ion density of the jth ion species and $N_{\rm e}$ is the electron density. For field aligned propagation, the location of the BB resonance corresponds to a cutoff condition for a reflected wave packet and leads to wave reflection and bouncing between BB resonance locations [*Rauch and Roux*, 1982; *Johnson et al.*, 1995; *Horne and Thorne*, 1997; *Johnson and Cheng*, 1999]

The other interesting ion-ion effect is the crossover frequency ($\omega_{\rm cr}$), where the R and L modes cross each other in the dispersion relation, which is given by

$$\omega_{\rm cr}^2 = \eta_1\omega_{\rm c2}^2 + \eta_2\omega_{\rm c1}^2. \tag{2}$$

For oblique propagation, the sense of polarization changes for a wave when its frequency crosses near the crossover value in a slowly varying medium. In the ionosphere, this polarization reversal provides the mechanism by which upgoing electron whistlers can become proton whistlers [*Gurnett et al.*, 1965].

When $\omega \ll \omega_{\rm ce}, \omega_{\rm pe}$, where $\omega_{\rm ce}$ and $\omega_{\rm pe}$ are the electron gyro- and plasma frequencies, the basic description of the plasma wave is given by the approximate cold plasma dispersion relation

$$n_\perp^2 \cong \frac{(R - n_\parallel^2)(L - n_\parallel^2)}{(S - n_\parallel^2)}, \tag{3}$$

where $n_\parallel$ and $n_\perp$ are refractive indices parallel and perpendicular to B_0, respectively. R, L and S are the tensor elements for two ions [*Johnson et al.*, 1995],

$$R(L) \cong \pm\frac{c^2}{V_{\rm A}^2}\frac{\omega_{\rm c1}\omega_{\rm c2}}{\omega_{\rm cut}}\frac{(\omega \pm \omega_{\rm cut})}{(\omega \pm \omega_{\rm c1})(\omega \pm \omega_{\rm c2})}, \tag{4}$$

$$S \cong \frac{c^2}{V_{\rm A}^2}\frac{\omega_{\rm c1}^2\omega_{\rm c2}^2}{\omega_{\rm bb}^2}\frac{(\omega^2 - \omega_{\rm bb}^2)}{(\omega^2 - \omega_{\rm c1}^2)(\omega^2 - \omega_{\rm c2}^2)}, \tag{5}$$

where V_A and ω_{cut} are the Alfvén velocity and the cutoff frequency for $R = 0$ or $L = 0$, respectively.

This approximate dispersion relation has a resonance when $n_\perp \to \infty$ and two cutoffs when $n_\perp \to 0$. The resonance condition is determined from (3),

$$n_\parallel^2 = S, \tag{6}$$

and the cutoff conditions are

$$n_\parallel^2 = R(L). \tag{7}$$

The resonance in (6) is the IIH resonance, and the frequency determined by (6) is an IIH resonance frequency (ω_{ii}). In two fluid plasmas or below the heaviest ion gyrofrequency in multi-ion plasmas, this resonance reduces to the Alfvén resonance (or the perpendicular ion cyclotron resonance) [*Karney et al.*, 1979; *Stix*, 1992],

$$\omega_A^2 = \frac{k_\parallel^2 V_A^2}{1 + k_\parallel^2 V_A^2/\omega_{pH}^2}, \tag{8}$$

where ω_{pH} is the proton plasma frequency. In the MHD approximation, Eq. (8) is reduced to $\omega_A = k_\parallel V_A$.

Figure 1 shows the $n_\perp^2$ dispersion relation using Eq. (3) in an electron-proton-sodium plasma for (a) $\omega < \omega_{cNa}$ and (b) $\omega_{cNa} < \omega < \omega_{cH}$. When a wave frequency is lower than the heaviest ion gyrofrequency, this wave mode has one resonance which corresponds the Alfvén resonance and one cutoff in Figure 1(a). This wave is referred to as Class I following *Rauch and Roux* [1982]. In this case where $\omega = 0.69\omega_{cNa} = 0.03\omega_{cH}$, regions for $\eta_{Na} < 0.074$ or $\eta_{Na} > 0.28$ are wave stop gaps and the waves cannot propagate. However, if the spatial width of stop gaps is smaller than the incident wavelength, significant wave energy can tunnel through this region.

In Figure 1 (b) there are two different wave modes for $\omega_{cNa} < \omega < \omega_{cH}$. Waves referred to as Class II appear on the H^+-rich plasma side (right side in Figure 1). This mode has a cutoff when η_{Na} increases. The waves that appear on the Na^+-rich side of the plasma are referred to as Class III and have the IIH resonance. In between the IIH resonance and the Class II cutoff, there is a wave stop gap.

The resonant absorption at the IIH resonance can occur for incident waves from either the H^+-rich or Na^+-rich sides. Waves launched at H^+-rich plasma in Figure 1(b) propagate obliquely to $\mathbf{B}_0$ as R-X wave and encounter the crossover region first. When $\omega = \omega_{cr}$, the polarization reversal occurs and waves propagate as an L-X wave. However when $k_\perp \gg k_\parallel$, this wave is mostly linearly polarized for both the L-X and R-X waves. If the wavelength is large enough so that the wave can tunnel through the stop gaps, energy transfer to the IIH resonance occurs. Because there is no cutoff or stop gap on the Na^+-rich plasma side, the wave launched at the left side is transferred into the IIH resonance directly. *Lee et al.* [2008] calculated the mode conversion efficiencies from the incident waves from H^+- and He^+-rich plasmas to the IIH resonance for incident waves, respectively. They showed that the absorption from Class II to the IIH resonance variation becomes perfect if the stop gap is sufficiently large, while the mode conversion efficiency from the Class II is nearly zero unless the stop gap is small.

When an incident compressional wave satisfies the resonance condition in Eq. (6), the resonant absorption for $\omega_{cNa} < \omega < \omega_{cH}$ occurs as shown in Figure 1(b), except at the crossover frequency. For $\omega = \omega_{cr}$, the dispersion relation in Eq. (3) is reduced to

$$n^2 = S\,|_{\omega=\omega_{cr}}, \tag{9}$$

where $n^2 = n_\parallel^2 + n_\perp^2$ and $S = L = R\,|_{\omega=\omega_{cr}}$. Thus, for $\omega = \omega_{cr}$ (or the location where $S = R = L$), there is no resonant absorption or mode conversion in multi-ion plasmas, and wave propagates through the crossover region.

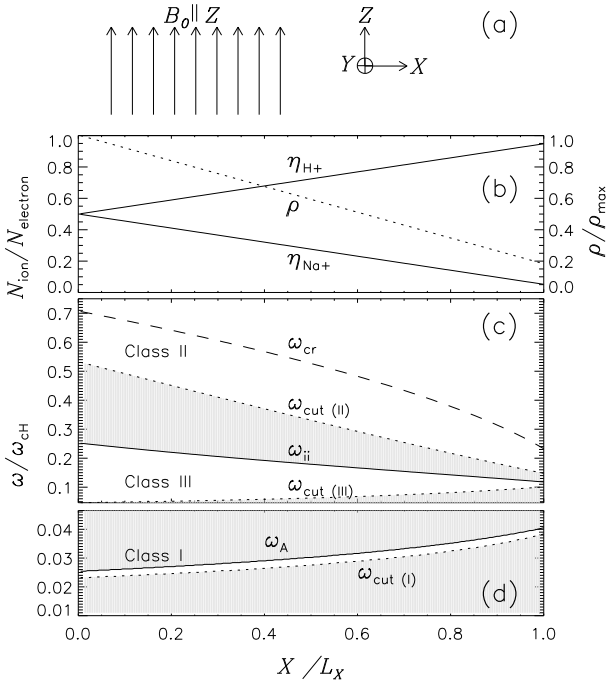

Figure 2. (a) Schematic illustration of the simulation. The inhomogeneity and $\mathbf{B}_0$ lie in the X and Z directions, respectively, and an impulsive input is assumed at $X = 0$. (b) The proton ($\eta_H = N_H/N_e$) and sodium density ratio ($\eta_{Na} = N_{Na}/N_e$) are shown as a function of X, and are consistent with previous estimated sodium density ratio 0.1 to 1.0 [*Ip*, 1986; *Cheng et al.*, 1987]. The critical frequencies: cutoff (ω_{cut}), crossover (ω_{cr}), ion-ion hybrid resonance (ω_{ii}) and Alfvén resonance (ω_A) frequencies for (c) $\omega_{cNa} < \omega < \omega_{cH}$ and (d) $\omega < \omega_{cNa}$. There are three cutoffs for Class I, II and III, $\omega_{cut(I)} < \omega_A$, $\omega_A < \omega_{cut(III)} < \omega_{ii}$ and $\omega_{cut(II)} > \omega_{ii}$. The shaded regions represent frequency stop-bands where the wave is evanescent.

3. Numerical Model

In order to consider Mercury's multi-ion plasmas, we employ the numerical model which has been developed by *Kim and Lee* [2003]. In cold plasmas, it solves the linearized Maxwell equations, the electron momentum and continuity equations, and Ohm's law for a single particle of species j:

$$\nabla \times \mathbf{E} = -\frac{\partial \mathbf{B}}{\partial t}, \tag{10}$$

$$\nabla \times \mathbf{B} = \mu_0 \mathbf{J} + \frac{1}{c^2}\frac{\partial \mathbf{E}}{\partial t}, \tag{11}$$

$$N_j m_j \frac{\partial \mathbf{v}_j}{\partial t} = N_j q_j (\mathbf{E} + \mathbf{v}_j \times \mathbf{B}_0), \tag{12}$$

$$\mathbf{J} = \sum_j N_j q_j \mathbf{v}_j \tag{13}$$

where $\mathbf{E}$, $\mathbf{B}$, $\mathbf{v}$, and $\mathbf{J}$ are the perturbed electric and magnetic fields, velocity, and current density, respectively, and N_j and $\mathbf{B}_0$ are the background density and magnetic fields, respectively.

The following assumptions and model of Figure 2 are adopted to solve these equation numerically:

1. To see heavy ion effects easily, B_0 and N_e are assumed to be constants and typical values for the electron density $N_e = 3\text{cm}^{-3}$ and the background magnetic field strength $B_0 = 86\text{nT}$ [*Russell*, 1989] at Mercury are used. $\mathbf{B}_0$ lies in the Z direction and the inhomogeneity is introduced in the X direction in Figure 2(a).

2. Because proton and sodium ions are the main constituents at Mercury [*Ip*, 1986; *Cheng et al.*, 1987], we adopt an electron-proton-sodium plasma in our model. We assume a composition variation. Figure 2(b) plots the corresponding ion concentration profile for proton (η_H) and sodium (η_{Na}) and the mass density (ρ) where the box has a scale of $L_X = 10^3$ km in the radial direction of X. It is assumed that η_H increases and η_{Na} and ρ decreases when X increases. The sodium to proton density ratio (η_{Na}/η_H) is assumed 0.055 at $X = L_X$ and 1.0 at $X = 0$, respectively, which are consistent with previous estimated sodium to proton density ratios (0.1 to 1.0) [*Ip*, 1986; *Cheng et al.*, 1987].

3. We limit ourselves to harmonic variations in the Y and Z directions, and all waves are proportional to $\exp(ik_Y Y + ik_Z Z)$, where k_Y and k_Z are the given Y and Z direction wavenumbers. k_Z is assumed to be a wavenumber fundamental oscillation on a field line length of 4,000 km [*Russell*, 1989] and $k_Y = 2\pi/\lambda_Y$ where $\lambda_Y = 2\pi R_M$ and R_M is the radius of Mercury.

4. The impulsive input is excited by imposing an impulse in E_y at $X = 0$ during $0 \le t \le 2t_{cH}$, where $t_{cH} = 2\pi/\omega_{cH}$, which is similar to a compressional impulse used in previous MHD [e.g., *Lee and Lysak*, 1989] and two-fluid simulations [*Kim and Lee*, 2003]. The simulation is run from $t = 0$ to $t = 100t_{cH}$, which satisfies the time limit from the phase-mixing length which is calculated from

$$L_{ph} = 2\pi \left(t \frac{d\omega_{res}}{dx} \right)^{-1} > \triangle x, \tag{14}$$

where ω_{res} is the resonance frequency and $\triangle x$ is the maximum grid spacing [*Mann et al.*, 1995].

5. The boundaries become perfect reflectors after the impulsive stimulus ends. Thus the total energy in the box model will remain constant in time, which enables us to examine the energy transfer among different modes without consideration of energy loss from the system.

Figure 2(c)-(d) shows the critical frequencies, such as cutoff ω_{cut}, crossover ω_{cr}, ion-ion hybrid resonance ω_{ii}, and Alfvén resonance ω_A frequencies for (c) $\omega_{cNa} < \omega < \omega_{cH}$ and (d) $\omega < \omega_{cNa}$. Here the shaded region represents the wave stop gaps. In this figure, ω_{ii} decreases from 0.25 to 0.12 while ω_A increases from 0.025 to 0.04 as η_{Na} decreases from 0.5 to 0.05. There are three cutoffs for Class I, II and III in Figure 2, $\omega_{cut(I)} < \omega_A$, $\omega_A < \omega_{cut(III)} < \omega_{ii}$, and $\omega_{cut(II)} > \omega_{ii}$. For $\omega_{cNa} < \omega < \omega_{cH}$, Class II waves launched at $X = 0$ (Na^+-rich plasma), encounter the IIH resonance directly. But Class III waves propagate from $X = L_X$ (H^+-rich plasma) pass through cutoff, stop gap, and resonance as in Figure 2(b). When $\omega < \omega_{cNa}$, the stop gaps are wider than the wave propagation region. However, L_X is comparable to the wave length of this frequency range. Thus the wave energy impulse from both $X = 0$ and L_X can reach to the ω_A.

4. Resonant absorption at the IIH resonance

In this section, we discuss the wave spectra when the impulsive input is excited at $X = 0$ as shown in Figure 2. The time histories of electromagnetic fields at the IIH and the cavity resonance are also presented. Since we focus on the IIH and heavy ion effects, we compare the time histories at the IIH and cavity resonances only.

4.1. Wave Spectra of magnetic fields

The power spectra of electric and magnetic field components are obtained through the Fourier transform at each grid point on X. Figure 4 shows the spectra of magnetic field, where the amplitudes are represented by the degree of brightness after they are logarithmically scaled. In this figure the horizontal axis is in the X direction and the vertical axis is a normalized frequency ranges from 0 to 0.75. It is noted that spectra is divided at $\omega = \omega_{cNa}$ for clarity and has finer resolution at smaller ω.

In Figure 4, the transverse mode (B_Y) exhibits the strong continuous spectrum of resonances from 0.12 to 0.25 between two ion gyrofrequencies. These are impulsively excited by the broadband compressional source at $X = 0$. This continuous band corresponds to the IIH resonant condition in Figure 4(d). However, there is no wave power enhancement at the crossover as we expected in Section 2. The compressional components of B_X and B_Z also were seen for this band, but the power is relatively weak because $k_X \gg k_Y$, k_Z. Thus the resonances at the IIH location show linear polarization on the azimuthal meridian. It is noted that this polarization characteristic is similar to MHD standing waves.

Below ω_{cNa}, the second continuous band is shown which corresponds to the Alfvén resonance in Figure 4(d). Unlike IIH resonance, it shows a mixture of compressional and transverse components, which is similar to previous single-ion simulation results [*Kim and Lee*, 2003].

The compressional components B_X and B_Z show the compressional cavity mode in Figure 4(a) and (c). Where

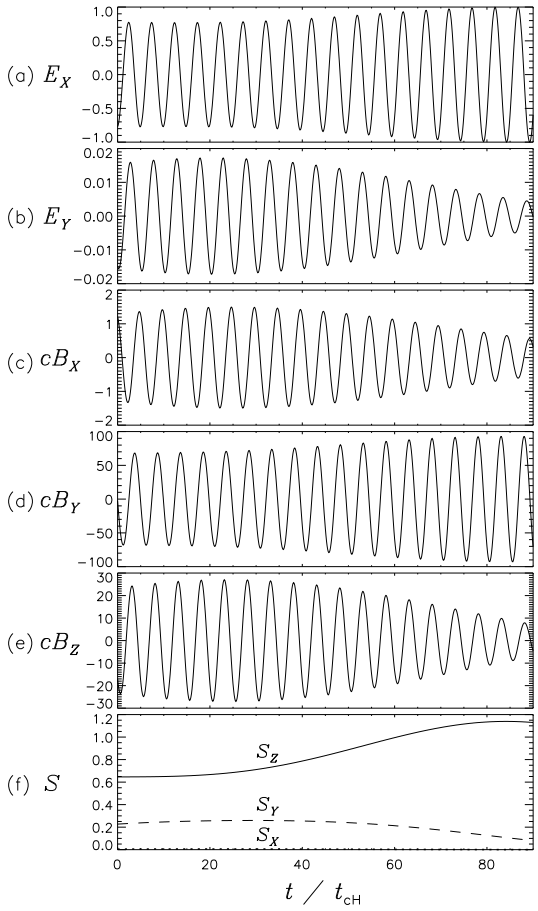

Figure 3. (a)-(c) Time histories of electromagnetic fields and (f) the Poynting flux $\mathcal{S}$ of wave at the IIH resonance marked as diamond for $\omega/\omega_{cH} = 0.2$. In (f), The dotted, dashed and solid lines are $\mathcal{S}_X$, $\mathcal{S}_Y$ and $\mathcal{S}_Z$, respectively.

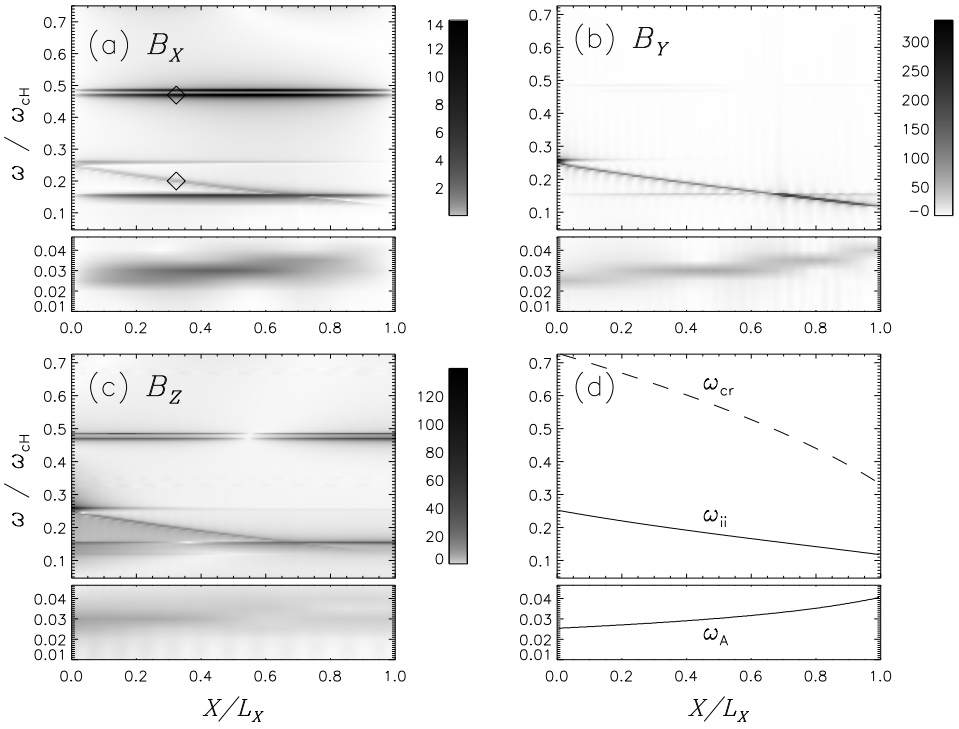

Figure 4. (a)-(c) The wave spectra of the perturbed magnetic field. The horizontal axis is the direction of inhomogeneity, X, and the vertical axis is a normalized frequency that ranges from 0 to 0.045 and 0.045 to 0.75. The vertical axis scale is different in the upper and bottom panels for clarity because the large mass difference between Na^+ and H^+ compresses the low frequency dispersion. The diamonds mark the point chosen for time histories. Here, B_Y is transverse component and B_Z represents pure compressional modes. (d) The calculated IIH, Alfvén continua which are clearly excited in the transverse B_Y component, and the crossover frequency.

the compressional cavity mode and the IIH resonance have the same frequency near $X = 0.0$ and $0.6 \leq X \leq 1.0$, it is evident that this transverse mode becomes relatively strong because of the coupling between the two modes. The detailed characteristics are described in Section 4.2 and 4.3.

We also examined a simulation with an impulsive input at $X = L_X$ (not shown in this paper). The characteristics of spectra are almost same as Figure 3: B_Y spectrum is strongly enhanced at the IIH resonance while the B_X and B_Z spectrum are dominant to cavity modes. However, the power the of the IIH resonance is much lower than Figure 3, which is expected from analytic calculations from *Lee et al.* [2008].

4.2. Wave properties at the IIH resonance

In order to examine the coupling properties between the compressional wave and the resonance, we select one resonant point $X/L_X = 0.32$ at a certain IIH frequency $\omega/\omega_{cH} = 0.2$ marked by diamond in Figure 4. Here ω_{ii} does not match any peak frequencies of the cavity modes, which enables us to avoid the effect of cavity modes.

Figure 3 shows time histories of $\mathbf{E}$ and $c\mathbf{B}$ at this resonant point which are obtained by applying the inverse Fourier transform. $\mathbf{E}$ and $c\mathbf{B}$ are normalized to an arbitrary value E_A which is the maximum value of E_X. In this figure, the E_X and B_Y components grow in time, while the other wave E_Y, B_X, and B_Z components damp. Therefore, our results show clearly that the compressional waves are mode converted into IIH waves near the IIH region $\omega \approx \omega_{ii}$. It should be noted that the resonant mode absorption characteristics are similar to MHD resonant absorption.

To examine wave energy flow, the Poynting flux, $\mathcal{S}$, is calculated and plotted in Figure 3 (f). In this figure, $\mathcal{S}_Z$ is dominant, and it is evident that the IIH resonance is strongly guided by B_0. Thus the IIH resonance as well as the Alfvén resonance can be a mechanism of FLR in the multi-ion plasmas. However, the spectral characteristics of the waves shown in Figure 4 are opposite to the spectral feature of the ULF waves observed at Mercury [*Russell*, 1989] where B_X and B_Z are dominant and B_Y is less dominant. This means the observed waves are not likely FLRs.

4.3. Wave properties at the cavity resonance

Figure 5 shows the time histories of the cavity modes. In contrast to the results shown in Figure 3, the wave mode has dominant E_Y, B_X and B_Z components. In this figure, all components increase in time. This growth represents wave superposition and there is no energy transferred between different wave modes. The wave energy flows obliquely to the $\mathbf{B}_0$ in Figure 5(f) and $\mathcal{S}_\perp \gg \mathcal{S}_\parallel$.

Conversely in Figure 3, the field aligned component, B_Z, shows the strongest power in Figure 5(e) and the power of transverse component B_Y is comparable to B_X, but $|B_Y| < |B_X|$. Thus the wave likely lies at the X-Z plane, which is similar to the wave observations at Mercury presented by *Russell* [1989]. However, the observed polarization state changed after the time period of the pulsation [*Russell*, 1989]. If we ignore B_Y, the power ratio $|B_X/B_Z|$ is proportional to $|k_Z/k_X|$. In this case, $k_X > k_Z$ and $B_X < B_Z$. The propagation direction and the magnetic field ratio of compressional waves, $|B_X/B_Z|$, can be changed by the plasma conditions (e.g., $k_X \sim \omega/V_A - k_Z$ as the density and Alfvén velocity vary). On the other hand for the transverse mode converted wave, at the IIH resonance, B_Y is always much greater than B_X and B_Z and is not very sensitive to $|k_Y/k_Z|$. Thus the observation of variable polarizations for the observed waves could be an evidence for a narrow band wave to be a compressional wave mode rather than FLR.

However, the wave in Figure 5 shows the phase difference between B_X and B_Z (B_Y) of about 90°, in contrast to the observations of 180°. This phase difference of 90° is due to the perfect boundary condition which requires a superposition of forward and backward propagating waves. In this simulation, the boundaries are assumed to be a perfect conductors, thus the normal component, B_X, and tangential component, B_Y and B_Z, have phase difference of 90°. However, in 2- or 3-D inhomogeneous unbounded plasmas, this phase difference could be changed.

5. Local Plasma Properties

Because the IIH resonance is the result of ion-ion effects, those frequencies are affected only by the relative ion density ratio rather than the absolute number density value. In this section, we examine methods to estimate the heavy ion ratio using the IIH and Alfvén resonances as FLRs at Mercury.

In electron-proton-sodium plasmas, $\eta_{\rm Na}$ can be derived as a function of observed wave frequency $\omega_{\rm obs}$ from Eq. (6),

$$\mathbf{A}\eta_{\rm Na} - \mathbf{B}k_\parallel^2 = \mathbf{C}, \quad (15)$$

$$\eta_{\rm H} + \eta_{\rm Na} = 1, \quad (16)$$

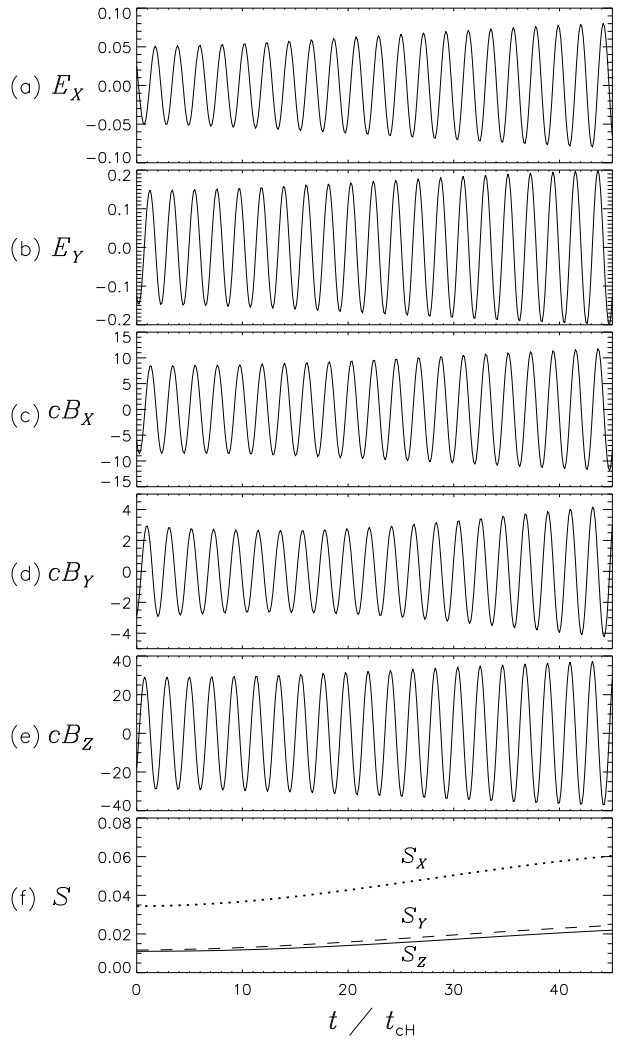

Figure 5. (a)-(c) Time histories of electromagnetic fields and (f) the Poynting flux $\mathcal{S}$ of wave at the cavity resonance marked as diamond for $\omega/\omega_{\rm cH} = 0.45$. In (f), The dotted, dashed and solid lines are $\mathcal{S}_X$, $\mathcal{S}_Y$ and $\mathcal{S}_Z$, respectively.

where

$$\mathbf{A} = \omega_{\rm pe}^2 \left(\frac{1}{\omega_{\rm obs}^2 - \omega_{\rm cH}^2} \frac{m_{\rm e}}{m_{\rm H}} - \frac{1}{\omega_{\rm obs}^2 - \omega_{\rm cNa}^2} \frac{m_{\rm e}}{m_{\rm Na}} \right), \quad (17)$$

$$\mathbf{B} = c^2/\omega_{\rm obs}^2, \quad (18)$$

$$\mathbf{C} = \omega_{\rm pe}^2 \left(\frac{1}{\omega_{\rm obs}^2 - \omega_{\rm cNa}^2} \frac{m_{\rm e}}{m_{\rm Na}} - \frac{1}{\omega_{\rm ce}^2} \right). \quad (19)$$

From Eq. (15)-(16), $\eta_{\rm H}$, $\eta_{\rm Na}$ and $k_\parallel$ can be estimated. There are two estimation methods: (1) to use one resonant wave assuming $k_\parallel$ and (2) to use two different observed resonance waves, the IIH and Alfvén resonances.

The field line length L_M at the observed wave location can be calculated from Mercury's magnetic field models [e.g., *Massetti et al.*, 2007]. If only one resonant wave is observed, by assuming $k_\parallel$ from L_M, $\eta_{\rm H}$ and $\eta_{\rm Na}$ can be estimated. In this case, for a field line length of 4,000 km, and if the FLR frequency is the same a the observed wave frequency of $\omega = 0.38\omega_{\rm cH}$, $\eta_{\rm Na}$ would be 0.74.

As shown in Figure 4, when broadband waves are excited, more than two resonances can occur at the same time in the multi-ion plasmas: the IIH and Alfvén resonances. When two resonant branches are observed, two sets of equations are obtained from Eq. (15). $k_\parallel$ as well as $\eta_{\rm H}$ and $\eta_{\rm Na}$ are calculated and L_M can also be estimated from $k_\parallel$. For example, assuming two observed frequencies of $\omega = 0.38\omega_{\rm cH}$ (as observed ULF wave) and $\omega = 0.038\omega_{\rm cH}$ in the proton-sodium plasmas, the density ratio $\eta_{\rm H}$ and $\eta_{\rm Na}$ and $k_\parallel$ can be estimated as $\eta_{\rm H} = 0.523$, $\eta_{\rm Na} = 0.477$ and $k_\parallel = 1.994 \times 10^{-3} {\rm km}^{-1}$, respectively. Using $k_\parallel$, the field line length also can be calculated to as $L_M = 1.576 \times 10^3$ km for the fundamental oscillation. This estimated L_M could be compared with L_M from Mercury's magnetic model.

The crossover and BB resonance also can used to estimate the ion density ratio from Eqs (1)-(2). *Othmer et al.* [1999] estimated the heavy ion population at Mercury using $\omega_{\rm cr}$. In the typical plasma parameters at Mercury, $\omega_{\rm ii} < \omega_{\rm cr}$ in Figure 2, thus their estimation of $\eta_{\rm Na}$ is lower than ours for same observed frequency. However, it should be noted that $\omega_{\rm cr}$ cannot be a FLR as shown in (6). *Lee et al.* [2008] also suggested that the monitoring the local heavy ion population is possible simply by examining peak frequencies of $\omega_{\rm bb}$ in Earth's magnetosphere.

6. Discussion and conclusion

In spite of the fact that the waves detected by the Mariner 10 spacecraft do not have the spectral feature of a pure standing Alfvén wave, several authors suggested that the observed waves are FLRs at Mercury [e.g., *Russell*, 1989; *Othmer et al.*, 1999] because they appeared in a narrow frequency band.

To examine FLRs at Mercury, we performed wave simulations in electron-proton- sodium plasmas. Our results show that the compressional cavity mode in Figure 4 and 5 are similar to the observed ULF waves, but the resonances in Figure 4 and 3 show opposite characteristics. Thus, the observed narrow band waves are likely compressional waves rather than a resonant wave mode. *Blomberg* [1997] and *Southwood* [1997] also argued that the observed waves cannot be pure standing Alfvén wave since they have compressional components and polarization in the X-Z meridian.

In multi-ion plasmas, there are two resonances which are guided along B_0, the Alfvén and IIH resonances. The IIH resonance can occur at the same spatial location as the Alfvén resonance but different frequency range: the Alfvén resonance occurs below the heaviest ion gyrofrequency and the IIH resonances are located between the ion gyrofrequencies. Our results in Figure 4 show that the wave converted

to the IIH resonance is strongly guided by the background magnetic field. The mode converted wave has similar characteristics to shear Alfvén waves in the Earth's magnetosphere. The time histories of electromagnetic fields in Figure 4 show that the transverse mode (E_X and B_Y) grows while other components damp. This behavior is evidence for the resonant absorption from compressional wave into the IIH resonance. Thus both of the Alfvén and IIH resonances can be a mechanism for FLR in Mercury's magnetosphere.

Othmer et al. [1999] suggested that when the resonance condition, Eq. (6), is satisfied at the crossover frequency, the FLR occurs in Mercury's magnetosphere. They assumed that the observed waves are FLRs at Mercury and focused on the linear polarization. Because at the crossover frequency location the group velocity of the guided mode is directed along B_0 for any direction of the wavevector [*Rauch and Roux*, 1982], they suggested that the crossover frequency is preferred to be the FLR in Mercury's magnetosphere. Although polarization reversal occurs at $\omega = \omega_{\rm cr}$, there is no resonance condition in Eq. (3) and no wave power enhancement in the wave spectra of the simulation (Figure 4). *Johnson and Cheng* [1999] and *Kim and Lee* [2005] showed that the numerical solutions of the polarization reversal left- (LH) to right-handed (RH) in the magnetosphere and RH to LH polarization in the ionosphere, respectively. Thus the polarization of ULF waves at Mercury can also change LH to RH or RH to LH at crossover region. But the crossover cannot provide a mechanism for FLRs at Mercury.

Finally, we introduce methods to estimate the heavy ion composition at Mercury's magnetosphere. Since Alfvén resonance and IIH resonance can occur simultaneously at the same location when there are broadband incoming compressional waves, it is expected that multiple resonances could be found at Mercury. If a spacecraft detects such resonant waves, the wave frequency could be used to estimate the local heavy ion density and elucidate the composition of Mercury's magnetosphere.

However, there are several limitations in our study. First, to examine the effect of variable ion concentration, we assumed a homogeneous magnetic field, B_0. But for inhomogeneous B_0, waves launched from low B_0 region can encounter the IIH resonance and the Alfvén resonance when they propagate into the strong B_0 region. Thus the absorption efficiencies at the Alfvén and IIH resonances should be different from that of homogeneous B_0 plasmas. It is necessary to investigate the Alfvén and the IIH resonances in inhomogeneous B_0 plasmas, such as a dipole coordinate system.

Second, a cold plasma model was adopted. *Southwood* [1997] pointed out that the observed wave could be similar to the terrestrial waves that are standing waves modified by the presence of hot plasmas. In hot plasma, incoming compressional waves can be converted into the slow ion Bernstein wave mode near the IIH resonance [e.g., *Jaeger et al.*, 2003]. Although we use a cold plasma model, resonant absorption at the IIH resonance is clearly shown in this paper, however, hot plasma effects should be considered.

Third, the geometry and/or density profile assumed was arbitrary. We neglected asymmetric effects, for convenience, which might be important in Mercury's magnetosphere [e.g., *Delcourt et al.*, 2003]. When a non-axisymmetric profile is assumed, it would become difficult to define the radial and azimuthal directions [*Lee et al.*, 2000]. These subjects will be left as future work.

In this paper, a numerical wave simulation in multi-ion plasmas was performed to investigate the FLR at Mercury. We found the following: (1) The observed ULF waves are likely compressional waves rather than FLR. (2) Resonant absorption occurs at the IIH resonance, thus incoming compressional waves are converted into the IIH resonance. (3) The IIH resonance is strongly guided by the background magnetic field and shows linear polarization in the east-west meridian. (4) Both the Alfvén and the IIH are suggested as a mechanism for FLR at Mercury. (5) The resonance frequency enables us to estimate the local heavy ion concentration ratio.

Acknowledgments. This work was supported by NASA grants (NNH04AB23I, NNH04AA73I, NNH04AA16I, NNG07EK69I, NNH07AF37I), NSF grant (ATM0411392), DOE Contract No. DE-AC02-76CH03073, and the Korea Research Foundation Grant funded by the Korean Government (KRF-2005-070-C00059).

References

Belmont, G., and L. Rezeau (2001), Magnetopause reconnection induced by magnetosheath Hall-MHD fluctuations, *J. Geophys. Res.*, *106*, 10,751–10,760, doi:10.1029/2000JA900151.

Blomberg, L. G. (1997), Mercury's magnetosphere, exosphere and surface: low-frequency field and wave measurements as a diagnostic tool, *Planet. Space Sci.*, *45*, 143–148.

Buchsbaum, S. J. (1960), Resonance in a plasma with two ion species, *Phys. Fluids*, *3*, 418–420.

Chen, L., and A. Hasegawa (1974), Plasma heating by spatial resonance of Alfvén wave, *Phys. Fluids*, *17*, 1399–1403.

Cheng, A. F., R. E. Johnson, S. M. Krimigis, and L. J. Lanzerotti (1987), Magnetosphere, exosphere, and surface of Mercury, *Icarus*, *71*, 430–440, doi:10.1016/0019-1035(87)90038-8.

Delcourt, D. C., S. Grimald, F. Leblanc, J.-J. Berthelier, A. Millilo, A. Mura, S. Orsini, and T. E. Moore (2003), A quantitative model of the planetary Na^+ contribution to Mercury's magnetosphere, *Ann. Geophys.*, *21*, 1723–1736.

Glassmeier, K.-H., P. N. Mager, and D. Y. Klimushkin (2003), Concerning ULF pulsations in Mercury's magnetosphere, *Geophys. Res. Lett.*, *30*, 4–1.

Glassmeier, K.-H., D. Klimushkin, C. Othmer, and P. Mager (2004), ULF waves at Mercury: Earth, the giants, and their little brother compared, *Adv. Space Res.*, *33*, 1875–1883, doi: 10.1016/j.asr.2003.04.047.

Gurnett, D. A., S. D. Shawhan, N. M. Brice, and R. L. Smith (1965), Ion Cyclotron Whistlers, *J. Geophys. Res.*, *70*, 1665.

Hasegawa, A., K. H. Tsui, and A. S. Assis (1983), A theory of long period magnetic pulsations. III - Local field line oscillations, *Geophys. Res. Lett.*, *10*, 765–767.

Horne, R. B., and R. M. Thorne (1997), Wave heating of He^+ by electromagnetic ion cyclotron waves in the magnetosphere: Heating near the H^+ - He^+ bi-ion resonance frequency, *J. Geophys. Res.*, *102*, 11,457–11,472, doi:10.1029/97JA00749.

Ip, W.-H. (1986), The sodium exosphere and magnetosphere of Mercury, *Geophys. Res. Lett.*, *13*, 423–426.

Jaeger, E. F., et al. (2003), Sheared Poloidal Flow Driven by Mode Conversion in Tokamak Plasmas, *Phys. Rev. Lett.*, *90*(19), 195,001, doi:10.1103/PhysRevLett.90.195001.

Johnson, J. R., and C. Z. Cheng (1999), Can ion cyclotron waves propagate to the ground?, *Geophys. Res. Lett.*, *26*, 671–674, doi:10.1029/1999GL900074.

Johnson, J. R., T. Chang, and G. B. Crew (1995), A study of mode conversion in an oxygen-hydrogen plasma, *Phys. Plasmas*, *2*, 1274–1284.

Karney, C. F. F., F. W. Perkins, and Y.-C. Sun (1979), Alfvén resonance effects on magnetosonic modes in large tokamaks, *Phys. Rev. Lett.*, *42*, 1621–1624, doi: 10.1103/PhysRevLett.42.1621.

Kim, E.-H., and D.-H. Lee (2003), Resonant absorption of ULF waves near the ion cyclotron frequency: A simulation study, *Geophys. Res. Lett.*, *30*(24), 3–1.

Kim, E.-H., and D.-H. Lee (2005), Simulation study of electron and proton whistlers in the Ionosphere, *J. Korean Phys. Soc.*, *46*(2), 541–545.

Klimushkin, D. Y., P. N. Mager, and K.-H. Glassmeier (2006), Axisymmetric Alfvén resonances in a multi-component plasma at finite ion gyrofrequency, *Ann. Geophys.*, *24*, 1077–1084.

Lammer, H., and S. J. Bauer (1997), Mercury's exosphere: origin of surface sputtering and implications, *Planet. Space Sci.*, *45*, 73–79.

Lee, D.-H., and R. L. Lysak (1989), Magnetospheric ULF wave coupling in the dipole model - The impulsive excitation, *J. Geophys. Res.*, *94*(A12), 17,097–17,103.

Lee, D.-H., R. L. Lysak, and Y. Song (2000), Field line resonances in a nonaxisymmetric magnetic field, *J. Geophys. Res.*, *105*, 10,703–10,712, doi:10.1029/1999JA000295.

Lee, D.-H., Johnson, J. R., K. Kim, and K.-S. Kim (2008), Effects of heavy ions on ULF wave resonances near the equatorial region, submitted to *J. Geophys. Res.*

Mann, I. R., A. N. Wright, and P. S. Cally (1995), Coupling of magnetospheric cavity modes to field line resonances: A study of resonance widths, *J. Geophys. Res.*, *100*, 19,441–19,456, doi:10.1029/95JA00820.

Massetti, S., S. Orsini, A. Milillo, and A. Mura (2007), Modelling Mercury's magnetosphere and plasma entry through the dayside magnetopause, *Planet. Space Sci.*, *55*, 1557–1568, doi:10.1016/j.pss.2006.12.008.

Mitchell, C., S. Vincena, J. Maggs, and W. Gekelman (2001), Laboratory observation of Alfvén resonance, *Geophys. Res. Lett.*, *28*, 923–926, doi:10.1029/2000GL012165.

Othmer, C., K.-H. Glassmeier, and R. Cramm (1999), Concerning field line resonances in Mercury's magnetosphere, *J. Geophys. Res.*, *104*(A5), 10,369–10,378, doi:10.1029/1999JA900009.

Rauch, J. L., and A. Roux (1982), Ray tracing of ULF waves in a multicomponent magnetospheric plasma - Consequences for the generation mechanism of ion cyclotron waves, *J. Geophys. Res.*, *87*, 8191–8198.

Rezeau, L., A. Morane, S. Perraut, A. Roux, and R. Schmidt (1989), Characterization of Alfvénic fluctuations in the magnetopause boundary layer, *J. Geophys. Res.*, *94*, 101–110.

Russell, C. T. (1989), ULF waves in the Mercury magnetosphere, *Geophys. Res. Lett.*, *16*, 1253–1256.

Smith, R. L., and N. Brice (1964), Propagation in Multicomponent Plasmas, *J. Geophys. Res.*, *69*, 5029.

Southwood, D. J. (1974), Some features of field line resonances in the magnetosphere, *Planet. Space Sci.*, *22*, 483–491, doi:10.1016/0032-0633(74)90078-6.

Southwood, D. J. (1997), The magnetic field of Mercury, *Planet. Space Sci.*, *45*, 113–117.

Stix, N. (1992), *Waves in plasmas*, American Institute of Physics, New York.

Tamao, T. (1965), Transmission and coupling resonance of hydromagnetic disturbances in the non-uniform Earths magnetosphere, *Sci. Rep. Tohoku Univ., Ser. 5, Geophys.*, *17*(2), 43.

Tsushima, A., Y. Amagishi, and M. Inutake (1982), Observations of spatial Alfvén resonance, *Phys. Lett. A*, *88*, 457–460.

Uberoi, C. (1972), Alfvén Waves in Inhomogeneous Magnetic Fields, *Physics of Fluids*, *15*, 1673–1675.

Winglee, R. M. (1982), Finite frequency effects on magnetosonic wave mode conversion , *Plasma Phys.*, *24*, 1161–1168.

Young, D. T., S. Perraut, A. Roux, C. de Villedary, R. Gendrin, A. Korth, G. Kremser, and D. Jones (1981), Wave-particle interactions near Ω_{He^+} observed on GEOS 1 and 2. I - Propagation of ion cyclotron waves in He^+-rich plasma, *J. Geophys. Res.*, *86*, 6755–6772.

E.-H. Kim and J. R. Johnson, Plasma Physics Laboratory, Princeton University, Princeton, NJ 08543 (e-mail:ehkim@pppl.gov)

D.-H. Lee, Department of Astronomy and Space Science, Kyung Hee University, Yongin, Kyunggi, 449-701 Korea

The Princeton Plasma Physics Laboratory is operated
by Princeton University under contract
with the U.S. Department of Energy.

Information Services
Princeton Plasma Physics Laboratory
P.O. Box 451
Princeton, NJ 08543

Phone: 609-243-2750
Fax: 609-243-2751
e-mail: pppl_info@pppl.gov
Internet Address: http://www.pppl.gov